

# Defending Against Image Corruptions Through Adversarial Augmentations

Dan A. Calian Florian Stimberg Olivia Wiles Sylvestre-Alvise Rebuffi  
András György Timothy Mann Sven Gowal

{dancalian, stimberg, oawiles, sylvestre, agyorgy, timothymann, sgowal}@google.com

DeepMind

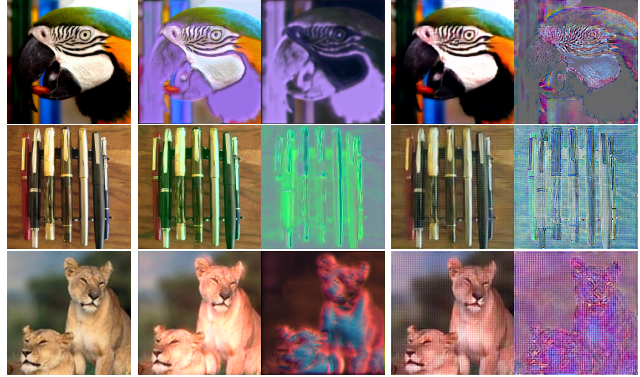
## Abstract

Modern neural networks excel at image classification, yet they remain vulnerable to common image corruptions such as blur, speckle noise or fog. Recent methods that focus on this problem, such as AugMix and DeepAugment, introduce defenses that operate in expectation over a distribution of image corruptions. In contrast, the literature on  $\ell_p$ -norm bounded perturbations focuses on defenses against worst-case corruptions. In this work, we reconcile both approaches by proposing AdversarialAugment, a technique which optimizes the parameters of image-to-image models to generate adversarially corrupted augmented images. We theoretically motivate our method and give sufficient conditions for the consistency of its idealized version as well as that of DeepAugment. Our classifiers improve upon the state-of-the-art on common image corruption benchmarks conducted in expectation on CIFAR-10-C and improve worst-case performance against  $\ell_p$ -norm bounded perturbations on both CIFAR-10 and IMAGENET.

## 1. Introduction

By following a process known as Empirical Risk Minimization (ERM) [60], neural networks are trained to minimize the average error on a training set. ERM has enabled breakthroughs in a wide variety of fields and applications [15, 31, 28], ranging from ranking content on the web [7] to autonomous driving [4] via medical diagnostics [11]. ERM is based on the principle that the data used during training is independently drawn from the same distribution as the one encountered during deployment. In practice, however, training and deployment data may differ and models can fail catastrophically. Such occurrence is commonplace as training data is often collected through a biased process that highlights confounding factors and spurious correlations [58, 32], which can lead to undesirable consequences (e.g., <http://gendershades.org>).

As such, it has become increasingly important to ensure that deployed models are robust and generalize to various input corruptions. Unfortunately, even small corruptions can



(a) Original (b) AdA (EDSR,  $\nu = .0375$ ) (c) AdA (CAE,  $\nu = .015$ )

Figure 1: **Adversarial examples generated using AdA attacks.** Examples are shown from two different backbone architectures as used by AdA: EDSR (b) and CAE (c). Original clean images are shown in (a); the image pairs in (b) and (c) show the adversarial example on the left and exaggerated differences on the right. In this case, AdA with either backbone introduces local and global color shifts, while AdA (EDSR) preserves high-frequency details and AdA (CAE) removes them. AdA (CAE) also introduces grid-like artifacts due to the transposed convolutions in the CAE decoder<sup>1</sup>.

significantly affect the performance of existing classifiers. For example, [49, 27] show that the accuracy of IMAGENET models is severely impacted by changes in the data collection process, while imperceptible deviations to the input, called adversarial perturbations, can cause neural networks to make incorrect predictions with high confidence [5, 6, 16, 33, 54]. Methods to counteract such effects, which mainly consist of using random or adversarially-chosen *data augmentations*, struggle. Training against corrupted data only forces the memorization of such corruptions and, as a result, these models fail to generalize to new corruptions [61, 14].

Recent work from [26] (also known as *AugMix*) argues that basic corruptions can be composed to improve the robustness of models to common corruptions. While the method performs well on average on the common corruptions present in CIFAR-10-C and IMAGENET-C, it generalizes poorly to

<sup>1</sup>For parity with previous work we use the same CAE architecture as in DeepAugment [24] which uses transposed convolutions instead of sub-pixel convolutions as in the original CAE model of [56].

the adversarial setting. Most recently, [34] proposed an adversarial training method based on bounding a neural perceptual distance (i.e., an approximation of the true perceptual distance), under the acronym of *PAT* for Perceptual Adversarial Training. Their method performs well against five diverse adversarial attacks, but, as it specifically addresses robustness to pixel-level attacks that directly manipulate image pixels, it performs worse than AugMix on common corruptions. In this work, we address this gap. We focus on training models that are robust to adversarially-chosen corruptions that preserve semantic content. We go beyond conventional *random data augmentation* schemes (exemplified by [26, 24]) and *adversarial training* (exemplified by [39, 17, 34]) by leveraging image-to-image models that can produce a wide range of semantically-preserving corruptions. Our contributions are as follows:

- We formulate an adversarial training procedure, named *AdversarialAugment* (or *AdA* for short), which is based on *DeepAugment* [24]. Instead of relying on heuristic operations as used in *DeepAugment*, our method finds adversarial examples by optimizing over the weights of pre-trained image-to-image models.
- We give sufficient conditions for the consistency of idealized versions of our method and *DeepAugment*, and provide PAC-Bayesian performance guarantees, following [42]. Our theoretical considerations highlight the potential advantages of *AdA* over *DeepAugment*, as well as the combination of the two. We also establish links to Invariant Risk Minimization (*IRM*) [1], Adversarial Mixing (*AdvMix*) [17] and Perceptual Adversarial Training [34].
- We improve upon the known state-of-the-art on CIFAR-10-C by achieving a mean corruption error (mCE) of **7.83%** when using our method *in conjunction* with others (vs. 23.51% for Perceptual Adversarial Training (PAT), 10.90% for AugMix and 8.11% for *DeepAugment*). The same combination of methods relying on *AdA* that performed best on CIFAR-10 also yield the model most robust to common image corruptions on IMAGENET-C (among all evaluated models).
- On  $\ell_2$  and  $\ell_\infty$  norm-bounded perturbations we significantly improve upon *DeepAugment* and AugMix, while maintaining generalization performance on IMAGENET-v2 and slightly improving it on CIFAR-10.1.

## 2. Related Work

**Data augmentation.** Data augmentation has been shown to reduce the generalization error of standard (non-robust) training. For image classification tasks, random flips, rotations and crops are commonly used [22]. More sophisticated techniques such as *Cutout* [12] (which produces random occlusions), *CutMix* [69] (which replaces parts of an image with another) and *mixup* [71, 57] (which linearly interpolates

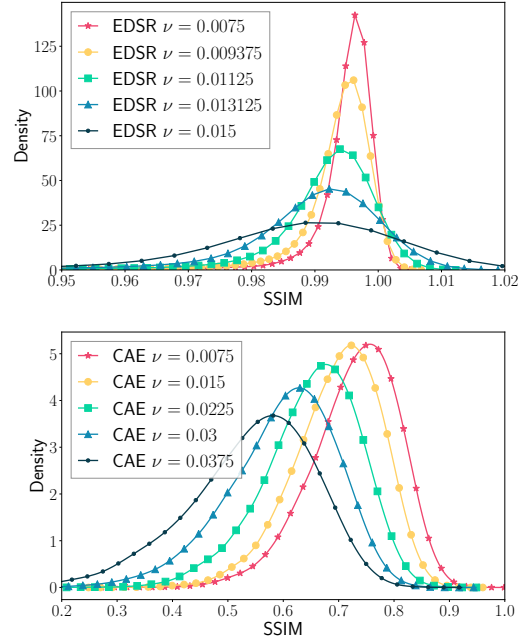


Figure 2: **Distribution of SSIM scores between clean and adversarial images found through *AdA*.** Densities are shown for both the *EDSR* (top) and *CAE* (bottom) backbones at five perturbation radii ( $\nu$ ). The *AdA* (*EDSR*) SSIM distribution with a low perturbation radius ( $\nu = 0.0075$ ) is highly concentrated around 0.99 yielding images very close to the clean inputs; increasing  $\nu$  slightly, dissipates density rapidly. For *AdA* (*CAE*) increasing the perturbation radius shifts the density lower, yielding increasingly more corrupted images. Also note that the SSIM range with non-zero support of *AdA* (*CAE*) is much wider than of *AdA* (*EDSR*).

between two images) all demonstrate extremely compelling results. [20] improved upon *mixup* by proposing an adaptive mixing policy. Works, such as *AutoAugment* [9] and related *RandAugment* [10], learn augmentation policies from data directly. These methods are tuned to improve standard classification accuracy and have been shown to work well on CIFAR-10, CIFAR-100, SVHN and IMAGENET. However, these approaches do not necessarily generalize well to larger data shifts and perform poorly on benign corruptions (e.g., blur or speckle noise) [55].

**Robustness to synthetic and natural data shift.** Several works argue that training against corrupted data only forces the memorization of such corruptions and, as a result, models fail to generalize to new corruptions [61, 14]. This has not prevented [13, 68, 26, 37, 24] from demonstrating that some forms of data augmentation can improve the robustness of models on IMAGENET-C, despite not being directly trained on these common corruptions. Most works on the topic focus on training models that perform well in expectation. Unfortunately, these models remain vulnerable to more drastic adversarial shifts [55].

**Robustness to adversarial data shift.** Adversarial data shift has been extensively studied [16, 33, 54, 40, 43, 39]. Most works focus on the robustness of classifiers to  $\ell_p$ -norm bounded perturbations. In particular, it is expected that a *robust* classifier be invariant to small perturbations in the pixel space (as defined by the  $\ell_p$ -norm). [16] and [39] laid down foundational principles to train robust networks, and recent works [72, 46, 50, 65, 18] continue to find novel approaches to enhance adversarial robustness. However, approaches focused on  $\ell_p$ -norm bounded perturbations often sacrifice accuracy on non-adversarial images [48]. Several works [2, 52, 66, 47, 63, 34] go beyond these analytically defined perturbations and demonstrate that it is not only possible to maintain accuracy on non-adversarial images but also reduce the effect of spurious correlations and reduce bias [17]. Unfortunately, most aforementioned approaches perform poorly on CIFAR-10-C and IMAGENET-C.

### 3. Defense Against Adversarial Corruptions

In this section, we introduce *AdA*, our approach for training models robust to image corruptions through the use of adversarial augmentations. We also explain how our work relates to Invariant Risk Minimization (IRM) [1], Adversarial Mixing (AdvMix) [17] and PAT [34].

**Corrupted adversarial risk.** We consider a model  $f_\theta : \mathcal{X} \rightarrow \mathcal{Y}$  parametrized by  $\theta$ . Given a dataset  $\mathcal{D} \subset \mathcal{X} \times \mathcal{Y}$  over pairs of examples  $x$  and corresponding labels  $y$ , we would like to find the parameters  $\theta$  which minimize the *corrupted adversarial risk*:

$$\mathbb{E}_{(x,y) \sim \mathcal{D}} \left[ \max_{x' \in \mathcal{C}(x)} L(f_\theta(x'), y) \right] \quad (1)$$

where  $L$  is a suitable loss function, e.g. the 0-1 loss for classification, and  $\mathcal{C} : \mathcal{X} \rightarrow 2^{\mathcal{X}}$  outputs a corruption set for a given example  $x$ . For example, in the case of an image  $x$ , a plausible corruption set  $\mathcal{C}(x)$  could contain blurred, pixelized and noisy variants of  $x$ .

In other words, we seek the optimal parameters  $\theta^*$  which minimize the corrupted adversarial risk so that  $f_{\theta^*}$  is invariant to corruptions, i.e.  $\forall x' \in \mathcal{C}(x) : f_{\theta^*}(x') = f_{\theta^*}(x)$ . For example if  $x$  is an image classified to be a horse by  $f_{\theta^*}$ , then this prediction should not be affected by the image being slightly corrupted by camera blur, Poisson noise or JPEG compression artifacts.

**AdversarialAugment (AdA).** Inspired by *DeepAugment*, we use image-to-image models to generate augmented corrupted images. However, instead of making use of heuristically-defined editing operations, we optimize over the parameters of the image-to-image models directly. We dub these image-to-image models *corruption networks*. We experiment with both the super-resolution EDSR model [36]

and the compressive autoencoder (CAE) model [56], the same ones as used in *DeepAugment*.

Let  $c_\phi : \mathcal{X} \rightarrow \mathcal{X}$  be a *corruption network* with parameters  $\phi = \{\phi_i\}_{i=1}^K$  which acts upon clean examples by corrupting them. Here each  $\phi_i$  corresponds to the vector of parameters in the  $i$ -th layer, and  $K$  is the number of layers (in practice, we apply biases in separate layers). Let  $\delta = \{\delta_i\}_{i=1}^K$  be a weight perturbation set, so that a corrupted variant of  $x$  can be generated by  $c_{\{\phi_i + \delta_i\}_{i=1}^K}(x)$ . With a slight abuse of notation we shorten  $c_{\{\phi_i + \delta_i\}_{i=1}^K}$  to  $c_{\phi + \delta}$ . Clearly, using unconstrained perturbations can result in exceedingly corrupted images which have lost all discriminative information and are not useful for training. For example, if  $c_\phi$  is a multi-layer perceptron, trivially setting  $\delta_i = -\phi_i$  would yield fully-zero, uninformative, outputs. Hence, we restrict the corruption sets by defining a maximum relative perturbation radius  $\nu > 0$ , and define the corruption set of *AdA* as  $\mathcal{C}(x) = \{c_{\phi + \delta}(x) \mid \|\delta\|_{2,\phi} \leq \nu\}$ , where the norm  $\|\cdot\|_{2,\phi}$  is defined as  $\|\delta\|_{2,\phi} = \max_{i \in \{1, \dots, K\}} \|\delta_i\|_2 / \|\phi_i\|_2$ .

**Finding adversarial corruptions.** For a clean image  $x$  with label  $y$ , a corrupted adversarial example within a bounded corruption distance  $\nu$  is a corrupted image  $x' = c_{\phi + \delta}(x)$  generated by the corruption network  $c$  with bounded parameter offsets  $\|\delta\|_{2,\phi} \leq \nu$  which causes  $f_\theta$  to misclassify  $x$ :  $f_\theta(x') \neq y$ . Similarly to [39], we find an adversarial corruption by maximizing a surrogate loss  $\tilde{L}$  to  $L$ , e.g., the cross-entropy loss between the corrupted image predicted logits and its clean label. We optimize over the perturbation  $\delta$  to  $c$ 's parameters  $\phi$ :

$$\max_{\|\delta\|_{2,\phi} \leq \nu} \tilde{L}(f_\theta(c_{\phi + \delta}(x)), y). \quad (2)$$

We solve this optimization problem using projected gradient ascent to enforce that perturbations  $\delta$  lie within the feasible set  $\|\delta\|_{2,\phi} \leq \nu$ . Examples of corrupted images obtained by *AdA* are shown in Figure 1.

**Adversarial training.** Given the model  $f$  parametrized by  $\theta$ , minimizing the corrupted adversarial risk from Equation 1 results in parameters  $\theta^*$  obtained by solving the following optimization problem:

$$\theta^* = \arg \min_{\theta} \mathbb{E}_{(x,y) \sim \mathcal{D}} \left[ \max_{\|\delta\|_{2,\phi} \leq \nu} \tilde{L}(f_\theta(c_{\phi + \delta}(x)), y) \right]. \quad (3)$$

**Meaningful corruptions.** A crucial element of *AdA* is setting the perturbation radius  $\nu$  to ensure that corruptions are varied enough to constitute a strong defense against common corruptions, while still being meaningful (i.e., without destroying semantics). We measure the extent of corruption induced by a given  $\nu$  through the structural similarity index measure (SSIM) [62] between clean and corrupted images. We plot the distributions of SSIM over various perturbation radii in Figure 2 for corrupted images produced by *AdA* on

CIFAR-10. We find that a perturbation radius of  $\nu = .015$  (for both corruption functions) yields enough variety in the corruptions (which is demonstrated for *EDSR* by having a large SSIM variance compared to, e.g.,  $\nu = 0.009375$ ) without destroying semantic meaning (having a high mean SSIM). We guard against unlikely but too severe corruptions (i.e. with too low SSIM) using an efficient approximate line-search procedure (details in appendix).<sup>2</sup> For CIFAR-10, we only found *EDSR* to be helpful and set the SSIM threshold at 0.3; for IMAGENET, we use both corruption functions and an SSIM threshold of 0.7.

**Relationship to DeepAugment & AugMix.** AugMix is a data augmentation method which stochastically composes standard image operations which affect color (e.g., posterize, equalize, etc.) and geometry (e.g., shear, rotate, translate) [26]. Classifiers trained with AugMix excel at robustness to image corruptions, and AugMix (when used with a Jensen-Shannon divergence consistency loss) sets the known state-of-the-art on CIFAR-10-C of 10.90%.

DeepAugment is a data augmentation technique introduced in [24]. This method creates novel image corruptions by passing each clean image through an image-to-image network (*EDSR* or *CAE*) while distorting the network’s internal parameters as well as intermediate activations. An extensive range of heuristic operations (9 for *CAE* and 17 for *EDSR*) are stochastically applied to the internal parameters, including: transposing, negating, zero-ing, scaling and even convolving (with random convolutional filters) parameters randomly. Activations are similarly distorted; for example, random dimensions are permuted or scaled by random Rademacher or binary matrices. Despite this complexity, classifiers trained with DeepAugment (with AugMix) set the known state-of-the-art mCE on IMAGENET-C of 53.6%.

Similarly to both AugMix and DeepAugment, *AdA* is also “specification-agnostic”, i.e., all three methods can be used to train classifiers to be robust to corruptions which are not known in advance (e.g., CIFAR-10-C, IMAGENET-C). Both DeepAugment and *AdA* operate by perturbing the parameters of image-to-image models. DeepAugment constrains parameter perturbations to follow specific user-defined directions (i.e., defined heuristically); *AdA* bounds their magnitude and prevents severe distortion (by approximately constraining the minimum SSIM deviation of the corrupted examples). To be able to define heuristic operations, DeepAugment relies on in-depth knowledge of the internals of the image-to-image models it employs; *AdA* does not. Instead, it relies on a global scalar threshold  $\nu$  to specify the amount of allowed parameter perturbation. AugMix requires having access to a palette of pre-defined useful input transformations; *AdA* requires access to a parameterized auto-encoding function (to use as a corruption function). As a result, we envision

<sup>2</sup>A similar approach for restricting the SSIM values of the samples during adversarial training was used in [21].

*AdA* to be more easily applicable to other domains, e.g., by leveraging auto-encoding models for audio signals [59] or text [44].

**Relationship to Invariant Risk Minimization.** IRM proposed by [1] considers the case where there are multiple datasets  $D_e = \{x_i, y_i\}_{i=1}^n$  drawn from different training environments  $e \in \mathcal{E}$ . The motivation behind IRM is to minimize the worst-case risk

$$\max_{e \in \mathcal{E}} \mathbb{E}_{(x,y) \in D_e} [L(f_\theta(x), y)]. \quad (4)$$

In this work, the environments are defined by the different corruptions  $x'$  resulting from adversarially choosing the parameter offsets  $\delta$  of  $\phi$ . Given a dataset  $\{x_i, y_i\}_{i=1}^n$ , we can rewrite the *corrupted adversarial risk* shown in (1) as (4) by setting the environment set  $\mathcal{E}$  to

$$\mathcal{E} = \{\{c_{\phi+\delta}(x_i), y_i\}_{i=1}^n \mid \|\delta\|_{2,\phi} \leq \nu\}. \quad (5)$$

This effectively creates an ensemble of datasets for all possible values of  $\delta$  for all examples. The crucial difference between IRM and *AdA* is in the formulation of the risk. In general, we expect *AdA* to be more risk-averse than IRM, as it considers individual examples to be independent from each other.

**Relationship to Adversarial Mixing.** [17] formulate a similar adversarial setup where image perturbations are generated by optimizing a subset of latents corresponding to pre-trained generative models. In this work, we can equivalently consider the parameters of our image-to-image models to be latents and could formulate AdvMix in the *AdA* framework. To the contrary of AdvMix, we do not need to rely on a known partitioning of the latents (i.e., disentangled latents), but do need to restrict the feasible set of parameter offsets  $\delta$ .

**Relationship to Perceptual Adversarial Training.** [34] directly optimizes input pixels and bound changes as to not exceed the perceptual distance (i.e., LPIPS [73]) between a original clean image and its corrupted variant. Their setup requires a complex machinery to project corrupted images back to the feasible set of images (within a fixed perceptual distance). *AdA*, by construction, uses a well-defined perturbation set and projecting corrupted network’s parameters is a trivial operation. This is only possible because perturbations are defined on weights/biases rather than input pixels.

## 4. Theoretical Considerations

In this section, we develop the conditions under which simplified versions of *AdA* and *DeepAugment* are consistent (i.e., as the data size grows, the expected error of the learned classifier over random corruptions converges to zero). The role of this section is two-fold: (1) to show that our algorithm is well-behaved (i.e., it converges), and (2) to introduce and to reason about the sufficient assumptions for convergence.

In this section, we assume  $f_\theta$  denotes a binary classifier (rather than a multi-class classifier), and that the family of functions  $\{f_\theta | \theta \in \Theta\}$  has a finite VC-dimension (which holds for the neural networks we consider, see, e.g., [3]). We also assume that  $\Phi$ , which parametrizes corruption functions, is a Euclidean vector space.

Before training or testing, the adversary selects a ground truth function  $f_{\theta^*}$  where  $\theta^* \in \Theta$  and an unknown probability measure  $\alpha(\Phi)$  over  $\Phi$  (of corruption functions). For any  $\theta \in \Theta$ , the corrupted adversarial risk is defined by

$$R(f_\theta, \alpha) = \mathbb{E}_{x \sim \mu(\cdot), \phi \sim \alpha(\cdot)} [L([f_\theta \circ c_\phi](x), f^*(x))] , \quad (6)$$

which is the expected risk of  $f_\theta$  composed with a random corruption function, and  $\mu$  is a probability measure over the input space.

Since  $\alpha$  is unknown, we cannot directly compute the corrupted adversarial risk. *DeepAugment* overcomes this problem by proposing a suitable replacement distribution  $\beta$  and instead scores classification functions by approximating  $R(f_\theta, \beta)$  (rather than  $R(f_\theta, \alpha)$ ). In contrast, *AdA* searches over a set, which we denote by  $\Phi_\beta \subset \Phi$  of corruptions to find the worst case, similar to adversarial training of [39].

**DeepAugment.** The idealized version of DeepAugment (which neglects optimization issues) is defined as

$$\hat{\theta}^{(n)} = \arg \min_{\theta \in \Theta} \frac{1}{n} \sum_{i=1}^n L([f_\theta \circ c_{\phi_i}](x_i), y_i) , \quad (7)$$

where  $\phi_i \sim \beta(\cdot)$  for  $i = 1, 2, \dots, n$ . The following assumption provides a formal description of a suitable replacement distribution.

**Assumption 1. (Corruption coverage)** *There exists a known probability measure  $\beta(\Phi)$  such that  $\alpha$  is absolutely continuous with respect to  $\beta$  (i.e.,  $\frac{\alpha(W)}{\beta(W)} < +\infty$  for all measurable subsets  $W \subseteq \Phi$ ) and for all  $x$ ,  $f_{\theta^*}(x) = f_{\theta^*}(c_\phi(x))$  for all  $\phi \in \text{ess sup}(\beta)$ , where  $\text{ess sup}(\beta)$  is the essential support of the distribution  $\beta$ .*

Assumption 1 says that while we do not know  $\alpha$ , we do know another distribution  $\beta$  over corruption functions and that  $\beta$  has support at least as broad as  $\alpha$ . Furthermore, any corruption functions sampled from  $\beta$  leave the ground truth label unchanged. Otherwise, there would exist a possible corruption where the adversary can change the ground truth label forcing any classifier to make a mistake.

Given Assumption 1, the problem reduces to learning under covariate shift and the principles of empirical risk minimization hold given that  $\theta^* \in \Theta$  [53, footnote 3]. Thus, the idealized version of DeepAugment is consistent.

**AdversarialAugment.** An idealized version of *AdA* is defined by

$$\hat{\theta}^{(n)} = \arg \min_{\theta \in \Theta} \frac{1}{n} \sum_{i=1}^n \sup_{\phi \in \text{ess sup}(\beta)} L([f_\theta \circ c_\phi](x_i), y_i) . \quad (8)$$

The supremum operation represents our ability to solve the difficult computational problem of finding the worst case corruption. Assuming that we can compute (8), the consistency of *AdA* is guaranteed by the fact that  $\theta^* \in \Theta$ . Furthermore, as the expected loss of the learned predictor converges to zero for the supremum loss (over the corruptions), so does  $R(f_{\hat{\theta}^{(n)}}, \beta)$ , and also  $R(f_{\hat{\theta}^{(n)}}, \alpha)$  since  $\text{ess sup}(\alpha) \subseteq \text{ess sup}(\beta)$  (based on Assumption 1).

**PAC-Bayesian analysis.** One can also argue about these algorithms using the PAC-Bayesian view. If random perturbations  $\epsilon$  are introduced to the parameter  $\theta$  of the classifier  $f_\theta$ , the following bound holds (see, e.g., [42]):<sup>3</sup> Given a prior distribution  $P$  over  $\Theta$ , which is independent of the training data, for any  $\eta \in (0, 1)$ , with probability at least  $1 - \eta$ ,

$$\begin{aligned} \mathbb{E}_\epsilon R(f_\theta, \alpha) & \\ & \leq \mathbb{E}_{\epsilon, \phi \sim \alpha(\cdot)} [\hat{R}(f_\theta)] + 4 \sqrt{\frac{\text{KL}(\theta + \epsilon \| P) + \log \frac{2n}{\eta}}{n}} \end{aligned} \quad (9)$$

where  $\hat{R}(f_\theta) = \frac{1}{n} \sum_{i=1}^n L([f_\theta \circ c_{\phi_i}](x_i), y_i)$  and  $\text{KL}(\theta + \epsilon \| P)$  is the KL divergence between the parameter distribution  $\theta + \epsilon$  (given  $\theta$ ) and  $P$ .<sup>4</sup> Defining  $P$  and  $\epsilon$  to have spherically invariant normal distributions with variance  $\sigma^2$  in every direction, the KL term becomes  $\frac{\|\theta\|_2^2}{2\sigma^2}$ , and so the second term goes to zero as the number of samples increases (and  $\theta$  does not grow fast). An even better choice, which we adopt in our experiments, is to choose the perturbation of each parameter to be proportional to the parameter value itself, by setting the standard deviation of  $\epsilon_j$  (the  $j$ th coordinate of  $\epsilon$ ) as  $\sigma_j = a\sigma|w_j| + b$ , making the KL term equal to  $\sum_j \frac{\theta_j^2}{2\sigma_j^2}$ . However, minimizing the first term on the right hand side of (9) is not straightforward during training, since we have no access to corruptions sampled from  $\alpha$ . DeepAugment tries to remedy this situation by using samples from  $\beta$ , however, the effectiveness of this depends on how well  $\beta$  approximates  $\alpha$ , more directly on the importance sampling ratios  $\alpha(W)/\beta(W)$  in Assumption 1. On the other hand, *AdA* minimizes the worst-case loss over  $\text{ess sup}(\beta)$ , which dominates the worst-case loss over  $\text{ess sup}(\alpha)$  under Assumption 1, which minimizes the expected loss over  $\alpha$ , which is the first term. Thus, *AdA* minimizes an upper bound on the first term, while DeepAugment only minimizes a proxy.<sup>5</sup>

<sup>3</sup>Experimental results presented in the appendix show that for various choices of the distribution of  $\epsilon$ , if the variance is small enough, the performance of the classifier only changes very slightly.

<sup>4</sup>To obtain this bound, one can think of the randomized classifier as the compound classifier  $f_\theta \circ c_\phi$  having parameters both  $\theta$  and  $\phi$ , and prior on  $\phi$  is  $\alpha$ , which then cancels from the KL term.

<sup>5</sup>Note that this is a calibrated proxy in the sense that the minimum of both the proxy and the original target is assumed at the same value  $\theta^*$ .

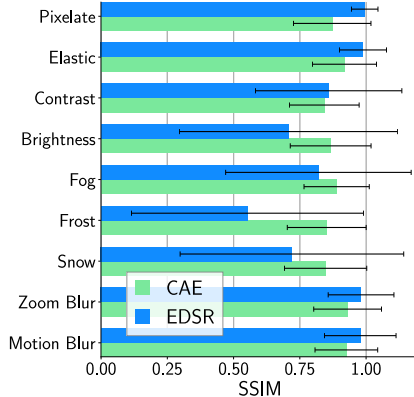


Figure 3: **Reconstructing CIFAR-10-C corruptions through *Ada* backbones.** These bar plots show the extent to which the *EDSR* and *CAE* models can be used to approximate the effects of 9 of the corruptions present in CIFAR-10-C. Bars show mean and std. dev. SSIM [62] (higher is better, 1 is max.) between pairs of corrupted images and their reconstructions through *EDSR/CAE*, optimized starting from the corresponding clean images.

**Discussion.** We have assumed that  $\theta^* \in \Theta$  implying that the classifier is over-parameterized. This is a common assumption in the literature which often holds in practice [70]. For parity with previous works that tackle robustness to image corruptions (like [24, 35, 51]) we constrain capacity and use the *ResNet50* architecture for all our models, but note that larger models can achieve better mCE: e.g., [24] train a very large model (RESNEXT-101  $32 \times 8d$  [67]) with AugMix and DeepAugment to obtain 44.5% mCE on IMAGENET-C.

In Figure 3 we explore how well Assumption 1 holds in practice, i.e., how well are the corruptions in CIFAR-10-C covered by the corruptions functions used in *Ada*. The figure shows how well 9 of the 15 corruptions present in the CIFAR-10-C benchmark can be approximated by the *EDSR* and *CAE* corruptions functions. For each image pair (of a corrupted and clean image) in a random 640-image subset of CIFAR-10-C and CIFAR-10, we optimize the perturbation to the corruption network parameters that best transform the clean image into its corrupted counterpart by solving  $\max_{\delta} \text{SSIM}(c_{\phi+\delta}(x), x') - 10^{-5} \|\delta\|_2^2$ , where  $\delta$  is the perturbation to the corruption network’s parameters,  $x$  is the clean example and  $x'$  is its corrupted counterpart. We use the Adam optimizer [29] to take 50 ascent steps, with a learning rate of 0.001. Finally, we average the residual SSIM errors across all five severities for each corruption type. Note that both models can approximate most corruptions well, except for *Brightness* and *Snow*. Some corruption types (e.g. *Fog*, *Frost*, *Snow*) are better approximated by *CAE* ( $0.84 \pm 0.16$  overall SSIM) while most are better approximated by *EDSR* ( $0.91 \pm 0.26$  overall SSIM).

## 5. Empirical Results

In this section we compare the performance of classifiers trained using our method (*Ada*) and competing state-of-the-art methods (AugMix [26], DeepAugment [24]) on (1) robustness to common image corruptions (on CIFAR-10-C & IMAGENET-C); (2) robustness to  $\ell_p$ -norm bounded adversarial perturbations; and (3) generalization to distribution shifts on other variants of IMAGENET and CIFAR-10. Omitted details and additional experimental results are presented in the appendix.

**Overview.** On CIFAR-10-C we set a new state-of-the-art mCE of 7.83% by combining<sup>6</sup> *Ada* with DeepAugment and AugMix. On IMAGENET (downsampled to  $128 \times 128$ ) with the same combination of methods we obtain 67.36% mCE which improves upon the best model from the literature that we train (70.05% mCE, using DeepAugment with AugMix). On both datasets, models trained with *Ada* gain non-trivial robustness to  $\ell_p$ -norm perturbations compared to all other models, while showing slightly better generalization to non-synthetic distribution shifts.

**Experimental setup.** For CIFAR-10 we train pre-activation *ResNet50* [23] models (as in [64]) on the clean training set of CIFAR-10 (and evaluate on CIFAR-10-C and CIFAR-10.1); our models employ  $3 \times 3$  kernels for the first convolutional layer, as in previous work [26]. For IMAGENET we train standard *ResNet50* classifiers on the training set of IMAGENET with standard data augmentation but  $128 \times 128$  re-scaled image crops (due to the increased computational requirements of adversarial training) and evaluate on IMAGENET- $\{C, R, v2\}$ . Results tables (Tables 1–4) contain only metrics from models we trained ourselves.

To be able to compare to DeepAugment on CIFAR-10 we generate augmented training samples ourselves using the authors’ code in two variants: one sample and ten samples per training example (indicated by “(10 $\times$ )” in the tables).

**Evaluation.** We summarize performance on corrupted image datasets using the mean corruption error introduced in [25]. mCE measures and aggregates top-1 classifier error across 15 corruption types and 5 corruption severities from IMAGENET-C and CIFAR-10-C. For a given corruption  $c$ , the corruption error across the five severities is  $E_c = \sum_{s=1}^5 E_{c,s}$ . For IMAGENET, the top-1 error for each corruption type and severity is weighted by the performance of an AlexNet classifier to give the normalized corruption error  $\bar{E}_c = E_c / E_c^{\text{AlexNet}}$ . This normalization corrects for corruption difficulty. The mCE is then the mean of the fifteen normalized corruption errors. For CIFAR-10, this AlexNet-relative correction is not applied, so the mean is taken over the unnormalized corruption errors  $E_c$ . We also report (absolute) top-1 error averaged across all severities for each individual corruption. For measuring robustness to  $\ell_p$ -norm

<sup>6</sup>We provide specifics on how we combine methods in the appendix.

bounded perturbations, on CIFAR-10 we attack our models with one of the strongest available combinations of attacks (AutoAttack & MultiTargeted as in [18]). For IMAGENET, we use a standard 100-step PGD attack with 10 restarts.

**Common corruptions.** On CIFAR-10, models trained with *AdA* (coupled with AugMix) obtain very good performance against common image corruptions, as shown in Table 1, excelling at *Digital* and *Weather* corruptions. Combining *AdA* with increasingly more complex methods results in monotonic improvements to mCE; i.e., coupling *AdA* with AugMix improves mCE from 12.49% to 8.80%; adding DeepAugment further pushes mCE to 8.58%. Finally, adding  $10\times$  more DeepAugment samples pushes mCE to 7.83% establishing a new state-of-the-art for CIFAR-10-C.

On IMAGENET, in Table 3 we see the same trend, where combining *AdA* with increasingly more methods results in similar monotonic improvements to mCE. The best method combination is the same as for CIFAR-10, which obtains 67.36% mCE. This constitutes an improvement of more than 15% mCE over nominal training and 2.69% mCE over the best non-*AdA* variant (DeepAugment + AugMix). These observations together indicate that the corruptions captured by *AdA* (by using both *EDSR* and *CAE*) complement the ones generated by both DeepAugment and AugMix.

On both datasets, achieving high performance on the three types of noise corruptions is most difficult for models trained with *AdA*. For example, on CIFAR-10, standalone *AdA* obtains very similar corruption errors on *Gaussian* and *Shot* noise as AugMix but lower error on most of the remaining corruptions. Compared to nominal training, *AdA* still helps w.r.t. noise corruptions, reducing mCE by approx. 25% on average, but not to the same extent as DeepAugment.

We can observe that *CAE* does not help with training robust models for CIFAR-10-C while it does help for IMAGENET-C. For example, training with *AdA* (*CAE*) and AugMix results in 19.09% mCE on CIFAR-10-C, adding *EDSR* as well brings the mCE to 9.95%; but the best results of 8.80% on CIFAR-10 (without DeepAugment) are obtained by using *EDSR* instead of *CAE*. We suspect this is because *CAE* removes high-frequency information, blurring images (see Figure 1 (c)) which results in severe distortions for the small  $32 \times 32$  images even at very small perturbation radii (see Figure 2).

**Adversarial perturbations.** For CIFAR-10, in the adversarial setting (Table 2) models trained with *AdA* perform best across all metrics; they gain a limited form of robustness to  $\ell_p$ -norm perturbations despite not training *directly* to defend against this type of attack. Interestingly, combining *AdA* with AugMix actually results in a drop in robustness across *all* five  $\ell_p$ -norm settings. However, combining with DeepAugment on top recovers the drop and increases robustness even more across four out of the five  $\ell_p$ -norm settings.

On IMAGENET, as shown in Table 4, the *AdA* variants that use *EDSR* obtain the highest robustness to  $\ell_p$ -norm adversarial perturbations; note that top-1 robust accuracy more than doubles from *AdA* (*CAE*) to *AdA* (*EDSR*) across all evaluated  $\ell_p$ -norm settings. As for CIFAR-10, combining the best *AdA* variant with DeepAugment results in the best  $\ell_p$  robustness performance.

By themselves, neither AugMix nor DeepAugment result in classifiers resistant to  $\ell_2$  attacks for either dataset (top-1 robust accuracies are close to 0% across the board), but the classifiers have non-trivial resistance to  $\ell_\infty$  attacks (albeit, much lower than *AdA* trained models). We believe this is because constraining the perturbations (in the  $\ell_2$ -norm) to weights and biases of the early layers of the corruption networks can have a similar effect to training adversarially with input perturbations (i.e., standard  $\ell_p$ -norm adversarial training). But note that *AdA* does not use any *input* perturbations.

**Generalization.** On CIFAR-10 (Table 2), interestingly, the two models trained with *AdA* alone or coupled with AugMix generalize (slightly) better than all other methods to CIFAR-10.1, with the best variant achieving 90.50% top-1 accuracy. Surprisingly, coupling *AdA* with DeepAugment reduces robustness in case of the natural distribution shift captured by CIFAR-10.1. Furthermore, including ten times more samples of DeepAugment results in even lower robust accuracy (over 2% more). This trend applies to IMAGENET results as well (Table 4); using DeepAugment jointly with *AdA* (+ AugMix) results in lower accuracy on IMAGENET-V2 than when just using *AdA* (+ AugMix). These observations uncover an interesting trade-off where the combination of methods that should be used depends on the preference for robustness to image corruptions vs. to natural distribution shifts.

## 6. Conclusion

We have shown that our method, *AdA*, can be used to defend against common image corruptions by training robust models, obtaining a new state-of-the-art mean corruption error on CIFAR-10-C. The same combination of methods relying on *AdA* that worked best for CIFAR-10 also yield the model most robust to common image corruptions on IMAGENET-C (among all models we evaluated). Models trained with *AdA* substantially improve upon both DeepAugment’s and AugMix’s performance on  $\ell_2$ - and  $\ell_\infty$ -norm bounded perturbations, while also having slightly improved generalization to natural distribution shifts. Our theoretical analysis provides sufficient conditions on the corruption-generating process to guarantee consistency of idealized versions of *AdA* and DeepAugment, and also highlights potential advantages of our method compared to DeepAugment, as well as that of the combination of the two methods. We hope our method will inspire future work into theoretically-supported methods for defending against common and adversarial image corruptions.

Table 1: **Robustness to common image corruptions (CIFAR-10-C)**. The table shows mean corruption error on CIFAR-10-C and individual corruption errors for each corruption type (averaged across all severities). We note that AugMix with an additional regularizing loss (JSD) and a ResNeXt architecture obtains 10.90% mCE [26] and sets the known state-of-the-art mCE on CIFAR-10-C prior to our result herein.

SETUP	MCE	NOISE			BLUR				WEATHER				DIGITAL			
		GAUSS	SHOT	IMPULSE	DROPCUTS	GLASS	MOTION	ZOOM	SNOW	FROST	FOG	BRIGHT	CONTRAST	ELASTIC	PIXEL	JPEG
<i>AdA</i> (EDSR) + DeepAugment (10×) + AugMix	<b>7.83%</b>	8.8	7.8	11.2	5.9	<b>10.7</b>	7.3	6.5	8.5	6.7	8.7	5.2	6.2	8.5	7.7	<b>7.8</b>
<i>AdA</i> (EDSR) + DeepAugment + AugMix	8.58%	9.8	8.7	12.4	6.3	11.6	8.0	6.8	9.4	7.5	8.1	5.4	6.8	9.2	9.7	8.6
<i>AdA</i> (EDSR) + AugMix	8.80%	16.4	12.8	14.1	5.7	10.4	7.5	6.3	<b>7.1</b>	6.1	6.4	<b>3.1</b>	<b>4.7</b>	<b>8.1</b>	11.9	8.4
<i>AdA</i> (EDSR)	12.49%	25.8	19.8	29.9	9.3	15.6	10.9	9.6	9.3	8.1	8.8	4.4	11.0	9.8	<b>6.9</b>	9.2
<i>AdA</i> (EDSR, CAE) + AugMix	9.95%	16.1	13.3	15.1	7.8	11.9	9.2	8.0	9.2	8.1	9.1	5.0	6.9	9.2	11.2	9.1
<i>AdA</i> (CAE) + AugMix	19.09%	19.1	17.6	22.4	15.8	22.3	18.4	16.8	21.1	19.1	24.4	15.4	19.3	18.8	19.6	16.5
DeepAugment	11.67%	12.1	10.2	15.2	7.1	20.3	12.3	8.4	12.3	9.8	9.3	6.7	13.1	11.8	14.1	12.2
DeepAugment + AugMix	10.15%	10.9	9.4	10.8	7.0	18.2	10.8	7.7	10.8	8.7	9.3	6.3	8.8	11.4	12.3	10.7
DeepAugment (10×)	8.30%	9.0	7.6	11.5	<b>5.4</b>	14.0	7.9	<b>6.1</b>	8.5	<b>6.6</b>	7.1	5.0	7.3	9.1	10.0	9.4
DeepAugment (10×) + AugMix	8.11%	<b>8.8</b>	7.7	<b>8.6</b>	5.7	14.1	7.9	6.2	8.1	6.1	7.3	5.1	6.8	9.2	10.4	8.9
AugMix	13.13%	26.2	18.3	10.6	7.2	32.5	10.8	9.0	10.3	10.1	<b>6.8</b>	4.7	6.1	11.4	20.1	13.0
Nominal	25.17%	58.8	44.6	49.1	15.1	44.7	19.3	19.1	15.6	17.9	10.6	5.3	17.2	15.3	24.7	19.8

Table 2: **Robustness to adversarial  $\ell_p$ -norm bounded perturbations and distribution shift (CIFAR-10)**. The table shows clean and robust top-1 accuracy against  $\ell_\infty$  and  $\ell_2$  attacks on CIFAR-10, and clean accuracy on CIFAR-10.1 (trained on the CIFAR-10 training set only).

SETUP	CLEAN	CIFAR-10.1	$\ell_2$		$\ell_\infty$		
			$\epsilon = 0.5$	$\epsilon = 1.0$	$\epsilon = 1/255$	$\epsilon = 2/255$	$\epsilon = 4/255$
<i>AdA</i> (EDSR) + DeepAugment (10×) + AugMix	94.93%	87.35%	<b>18.63%</b>	<b>0.99%</b>	77.72%	<b>49.95%</b>	<b>13.88%</b>
<i>AdA</i> (EDSR) + DeepAugment + AugMix	94.72%	88.20%	13.25%	0.30%	75.23%	44.78%	9.68%
<i>AdA</i> (EDSR) + AugMix	<b>96.26%</b>	<b>91.05%</b>	2.26%	0.00%	68.32%	26.45%	0.99%
<i>AdA</i> (EDSR)	96.18%	90.50%	8.61%	0.03%	<b>77.78%</b>	44.39%	5.89%
<i>AdA</i> (EDSR, CAE) + AugMix	95.36%	88.90%	5.96%	0.02%	67.88%	32.63%	3.90%
<i>AdA</i> (CAE) + AugMix	85.87%	74.30%	1.74%	0.01%	39.00%	12.77%	0.83%
DeepAugment	94.27%	87.10%	0.55%	0.00%	55.18%	14.43%	0.28%
DeepAugment + AugMix	94.25%	87.60%	0.56%	0.00%	49.63%	12.86%	0.15%
DeepAugment (10×)	95.57%	88.75%	1.56%	0.00%	64.72%	21.35%	0.70%
DeepAugment (10×) + AugMix	95.21%	89.35%	1.16%	0.00%	55.58%	17.07%	0.49%
AugMix	96.05%	90.40%	0.00%	0.00%	28.48%	1.53%	0.00%
Nominal	95.77%	89.65%	0.00%	0.00%	24.23%	0.85%	0.00%

Table 3: **Robustness to common image corruptions (IMAGENET-C 128×128)**. The table shows mean corruption error on IMAGENET-C and individual corruption errors for each corruption type (averaged across all severities). All results reported in this table correspond to models trained with 128 × 128 images. DeepAugment coupled with AugMix sets the known state-of-the-art mCE on IMAGENET-C with a ResNet50 of 53.6% [24].

SETUP	MCE	NOISE			BLUR				WEATHER				DIGITAL			
		GAUSS	SHOT	IMPULSE	DROPCUTS	GLASS	MOTION	ZOOM	SNOW	FROST	FOG	BRIGHT	CONTRAST	ELASTIC	PIXEL	JPEG
<i>AdA</i> (EDSR, CAE) + DeepAugment + AugMix	<b>67.36%</b>	<b>48.3</b>	<b>48.1</b>	<b>48.9</b>	62.7	65.7	60.3	63.0	55.9	<b>52.0</b>	44.0	36.1	44.1	56.0	<b>56.8</b>	44.8
<i>AdA</i> (EDSR, CAE) + AugMix	72.23%	61.6	61.1	64.7	66.0	69.0	60.3	60.3	58.0	55.8	41.2	33.4	<b>41.1</b>	54.0	60.3	60.2
<i>AdA</i> (EDSR) + AugMix	73.59%	67.3	68.2	71.7	65.6	73.8	62.8	61.1	61.3	58.7	39.6	<b>31.9</b>	43.2	55.6	60.8	48.5
<i>AdA</i> (CAE) + AugMix	80.85%	87.4	86.6	91.2	66.7	<b>65.3</b>	63.0	63.0	71.3	66.0	50.8	42.2	52.2	<b>53.5</b>	59.1	<b>44.6</b>
DeepAugment	73.04%	52.1	52.1	53.3	60.0	69.8	65.3	63.1	57.7	55.4	43.3	33.8	58.2	56.2	66.8	63.8
DeepAugment + AugMix	70.05%	50.5	50.0	51.5	<b>58.0</b>	67.8	<b>60.1</b>	<b>58.1</b>	<b>54.4</b>	53.3	<b>37.3</b>	33.4	43.6	56.8	64.2	72.0
AugMix	77.12%	70.4	71.6	75.8	67.2	75.1	64.4	59.8	60.9	61.1	37.9	34.7	46.9	57.5	71.4	55.9
Nominal	82.40%	73.2	74.8	80.1	71.4	78.5	70.8	65.4	66.1	63.6	46.1	35.8	63.3	57.4	72.4	55.9

Table 4: **Robustness to adversarial  $\ell_p$ -norm bounded perturbations and distribution shift (IMAGENET 128×128)**. The table shows clean and robust top-1 accuracy against  $\ell_\infty$  and  $\ell_2$  attacks on IMAGENET, and clean accuracy on IMAGENET-R and -v2.

SETUP	CLEAN	$\ell_2$		$\ell_\infty$		IMAGENET-R		IMAGENET-v2	
		$\epsilon = 0.5$	$\epsilon = 1.0$	$\epsilon = 1/255$	$\epsilon = 2/255$	TOP-1	TOP-5	TOP-1	TOP-5
<i>AdA</i> (EDSR, CAE) + DeepAugment + AugMix	67.25%	<b>36.64%</b>	<b>15.40%</b>	<b>12.07%</b>	<b>1.66%</b>	<b>27.43%</b>	<b>42.72%</b>	55.46%	79.00%
<i>AdA</i> (EDSR, CAE) + AugMix	71.44%	36.32%	14.40%	10.87%	1.25%	25.54%	40.20%	59.29%	81.72%
<i>AdA</i> (EDSR) + AugMix	74.28%	33.27%	10.85%	7.43%	0.66%	23.65%	37.94%	61.58%	83.71%
<i>AdA</i> (CAE) + AugMix	60.62%	15.67%	3.37%	1.09%	0.07%	21.17%	34.12%	49.28%	72.63%
DeepAugment	72.27%	17.75%	2.73%	0.44%	0.01%	21.67%	35.66%	60.50%	83.17%
DeepAugment + AugMix	71.56%	16.07%	2.44%	0.35%	0.01%	22.32%	36.76%	60.11%	82.92%
AugMix	74.24%	12.79%	1.84%	0.20%	0.01%	19.22%	32.59%	62.19%	84.18%
Nominal	<b>74.85%</b>	14.81%	2.31%	0.25%	0.01%	18.04%	30.83%	<b>62.97%</b>	<b>84.67%</b>



## References

- [1] Martin Arjovsky, Léon Bottou, Ishaan Gulrajani, and David Lopez-Paz. Invariant risk minimization. *arXiv preprint arXiv:1907.02893*, 2020. 2, 3, 4
- [2] Shumeet Baluja and Ian Fischer. Adversarial transformation networks: Learning to generate adversarial examples. *arXiv preprint arXiv:1703.09387*, 2017. 3
- [3] Peter L. Bartlett, Nick Harvey, Christopher Liaw, and Abbas Mehrabian. Nearly-tight VC-dimension and pseudodimension bounds for piecewise linear neural networks. *Journal of Machine Learning Research*, 20(63):1–17, 2019. 5
- [4] Mariusz Bojarski, Davide Del Testa, Daniel Dworakowski, Bernhard Firner, Beat Flepp, Praseem Goyal, Lawrence D. Jackel, Mathew Monfort, Urs Muller, Jiakai Zhang, Xin Zhang, Jake Zhao, and Karol Zieba. End to end learning for self-driving cars. *NIPS Deep Learning Symposium*, 2016. 1
- [5] Nicholas Carlini and David Wagner. Adversarial examples are not easily detected: Bypassing ten detection methods. In *Proceedings of the 10th ACM Workshop on Artificial Intelligence and Security*, pages 3–14. ACM, 2017. 1
- [6] Nicholas Carlini and David Wagner. Towards evaluating the robustness of neural networks. In *2017 IEEE Symposium on Security and Privacy*, 2017. 1
- [7] Paul Covington, Jay Adams, and Emre Sargin. Deep neural networks for YouTube recommendations. In *Proceedings of the 10th ACM Conference on Recommender Systems*, 2016. 1
- [8] Francesco Croce, Maksym Andriushchenko, Vikash Sehwal, Nicolas Flammarion, Mung Chiang, Prateek Mittal, and Matthias Hein. Robustbench: a standardized adversarial robustness benchmark, 2020. 14
- [9] Ekin D Cubuk, Barret Zoph, Dandelion Mane, Vijay Vasudevan, and Quoc V Le. Autoaugment: Learning augmentation policies from data. *IEEE Conf. Comput. Vis. Pattern Recog.*, 2019. 2
- [10] Ekin D. Cubuk, Barret Zoph, Jonathon Shlens, and Quoc V. Le. Randaugment: Practical automated data augmentation with a reduced search space. *IEEE Conf. Comput. Vis. Pattern Recog.*, 2020. 2
- [11] Jeffrey De Fauw, Joseph R Ledsam, Bernardino Romera-Paredes, Stanislav Nikolov, Nenad Tomasev, Sam Blackwell, Harry Askham, Xavier Glorot, Brendan O’Donoghue, Daniel Visentin, George van den Driessche, Balaji Lakshminarayanan, Clemens Meyer, Faith Mackinder, Simon Bouton, Kareem Ayoub, Reena Chopra, Dominic King, Alan Karthikesalingam, Cían O Hughes, Rosalind Raine, Julian Hughes, Dawn A Sim, Catherine Egan, Adnan Tufail, Hugh Montgomery, Demis Hassabis, Geraint Rees, Trevor Back, Peng T Khaw, Mustafa Suleyman, Julien Cornebise, Pearse A Keane, and Olaf Ronneberger. Clinically applicable deep learning for diagnosis and referral in retinal disease. In *Nature Medicine*, 2018. 1
- [12] Terrance DeVries and Graham W Taylor. Improved regularization of convolutional neural networks with dropout. *arXiv preprint arXiv:1708.04552*, 2017. 2
- [13] Robert Geirhos, Patricia Rubisch, Claudio Michaelis, Matthias Bethge, Felix A Wichmann, and Wieland Brendel. Imagenet-trained cnns are biased towards texture; increasing shape bias improves accuracy and robustness. In *International Conference on Learning Representations*, 2019. 2
- [14] Robert Geirhos, Carlos RM Temme, Jonas Rauber, Heiko H Schütt, Matthias Bethge, and Felix A Wichmann. Generalisation in humans and deep neural networks. In *Advances in Neural Information Processing Systems*, pages 7538–7550, 2018. 1, 2
- [15] Ian Goodfellow, Yoshua Bengio, and Aaron Courville. *Deep Learning*. MIT Press, 2016. 1
- [16] Ian J Goodfellow, Jonathon Shlens, and Christian Szegedy. Explaining and harnessing adversarial examples. *Int. Conf. Learn. Represent.*, 2015. 1, 3, 12
- [17] Sven Gowal, Chongli Qin, Po-Sen Huang, Taylan Cemgil, Krishnamurthy Dvijotham, Timothy Mann, and Pushmeet Kohli. Achieving Robustness in the Wild via Adversarial Mixing with Disentangled Representations. *arXiv preprint arXiv:1912.03192*, 2019. 2, 3, 4
- [18] Sven Gowal, Chongli Qin, Jonathan Uesato, Timothy Mann, and Pushmeet Kohli. Uncovering the limits of adversarial training against norm-bounded adversarial examples. *arXiv preprint arXiv:2010.03593*, 2020. 3, 7, 14
- [19] Priya Goyal, Piotr Dollár, Ross Girshick, Pieter Noordhuis, Lukasz Wesolowski, Aapo Kyrola, Andrew Tulloch, Yangqing Jia, and Kaiming He. Accurate, large mini-batch sgd: Training imagenet in 1 hour. *arXiv preprint arXiv:1706.02677*, 2017. 12
- [20] Hongyu Guo, Yongyi Mao, and Richong Zhang. Mixup as locally linear out-of-manifold regularization. In *Proceedings of the AAAI Conference on Artificial Intelligence*, 2019. 2
- [21] Muhammad Zaid Hameed. *New Quality Measures for Adversarial Attacks with Applications to Secure Communication*. PhD thesis, Imperial College London, 2020. 4
- [22] Kaiming He, Xiangyu Zhang, Shaoqing Ren, and Jian Sun. Deep residual learning for image recognition. *IEEE Conf. Comput. Vis. Pattern Recog.*, 2016. 2
- [23] Kaiming He, Xiangyu Zhang, Shaoqing Ren, and Jian Sun. Identity mappings in deep residual networks. In *European conference on computer vision*, pages 630–645. Springer, 2016. 6, 12
- [24] Dan Hendrycks, Steven Basart, Norman Mu, Saurav Kadavath, Frank Wang, Evan Dorundo, Rahul Desai, Tyler Zhu, Samyak Parajuli, Mike Guo, Dawn Song, Jacob Steinhardt, and Justin Gilmer. The Many Faces of Robustness: A Critical Analysis of Out-of-Distribution Generalization. *arXiv preprint arXiv:2006.16241*, 2020. 1, 2, 4, 6, 8, 12
- [25] Dan Hendrycks and Thomas Dietterich. Benchmarking neural network robustness to common corruptions and perturbations. *Proceedings of the International Conference on Learning Representations*, 2019. 6
- [26] Dan Hendrycks, Norman Mu, Ekin D. Cubuk, Barret Zoph, Justin Gilmer, and Balaji Lakshminarayanan. Augmix: A simple data processing method to improve robustness and uncertainty. *Int. Conf. Learn. Represent.*, 2020. 1, 2, 4, 6, 8, 12
- [27] Dan Hendrycks, Kevin Zhao, Steven Basart, Jacob Steinhardt, and Dawn Song. Natural adversarial examples. *arXiv preprint arXiv:1907.07174*, 2019. 1

- [28] Geoffrey Hinton, Li Deng, Dong Yu, George E Dahl, Abdelrahman Mohamed, Navdeep Jaitly, Andrew Senior, Vincent Vanhoucke, Patrick Nguyen, Tara N Sainath, and others. Deep neural networks for acoustic modeling in speech recognition: The shared views of four research groups. *IEEE Signal processing magazine*, 29(6):82–97, 2012. 1
- [29] Diederik P Kingma and Jimmy Ba. Adam: A method for stochastic optimization. *arXiv preprint arXiv:1412.6980*, 2014. 6
- [30] Klim Kireev, Maksym Andriushchenko, and Nicolas Flammarion. On the effectiveness of adversarial training against common corruptions, 2021. 14
- [31] Alex Krizhevsky, Ilya Sutskever, and Geoffrey E Hinton. ImageNet classification with deep convolutional neural networks. In *Adv. Neural Inform. Process. Syst.*, 2012. 1, 14
- [32] Andrey Kuehlikamp, Benedict Becker, and Kevin Bowyer. Gender-from-iris or gender-from-mascara? In *2017 IEEE Winter Conference on Applications of Computer Vision (WACV)*, pages 1151–1159. IEEE, 2017. 1
- [33] Alexey Kurakin, Ian Goodfellow, and Samy Bengio. Adversarial examples in the physical world. *ICLR workshop*, 2016. 1, 3, 12
- [34] Cassidy Laidlaw, Sahil Singla, and Soheil Feizi. Perceptual adversarial robustness: Defense against unseen threat models. In *International Conference on Learning Representations*, 2021. 2, 3, 4, 13, 14
- [35] Jungkyu Lee, Taeryun Won, Tae Kwan Lee, Hyemin Lee, Geonmo Gu, and Kiho Hong. Compounding the performance improvements of assembled techniques in a convolutional neural network, 2020. 6
- [36] Bee Lim, Sanghyun Son, Heewon Kim, Seungjun Nah, and Kyoung Mu Lee. Enhanced deep residual networks for single image super-resolution, 2017. 3
- [37] Raphael Gontijo Lopes, Dong Yin, Ben Poole, Justin Gilmer, and Ekin D. Cubuk. Improving robustness without sacrificing accuracy with patch gaussian augmentation. *arXiv preprint arXiv:1906.02611*, 2019. 2
- [38] Ilya Loshchilov and Frank Hutter. SGDR: stochastic gradient descent with warm restarts. In *Int. Conf. Learn. Represent.*, 2017. 12
- [39] Aleksander Madry, Aleksandar Makelov, Ludwig Schmidt, Dimitris Tsipras, and Adrian Vladu. Towards deep learning models resistant to adversarial attacks. *Int. Conf. Learn. Represent.*, 2018. 2, 3, 5
- [40] Seyed-Mohsen Moosavi-Dezfooli, Alhussein Fawzi, Jonathan Uesato, and Pascal Frossard. Robustness via curvature regularization, and vice versa. *IEEE Conf. Comput. Vis. Pattern Recog.*, 2019. 3
- [41] Yurii Nesterov. A method of solving a convex programming problem with convergence rate  $o(1/k^2)$ . In *Sov. Math. Dokl.*, 1983. 12
- [42] Behnam Neyshabur, Srinadh Bhojanapalli, David McAllester, and Nati Srebro. Exploring generalization in deep learning. In *Advances in Neural Information Processing Systems*, volume 30, 2017. 2, 5
- [43] Nicolas Papernot, Patrick McDaniel, Xi Wu, Somesh Jha, and Ananthram Swami. Distillation as a defense to adversarial perturbations against deep neural networks. *IEEE Symposium on Security and Privacy*, 2016. 3
- [44] Matthew Peters, Mark Neumann, Mohit Iyyer, Matt Gardner, Christopher Clark, Kenton Lee, and Luke Zettlemoyer. Deep contextualized word representations. In *Proceedings of the 2018 Conference of the North American Chapter of the Association for Computational Linguistics: Human Language Technologies, Volume 1 (Long Papers)*, pages 2227–2237, New Orleans, Louisiana, June 2018. Association for Computational Linguistics. 4
- [45] Boris T Polyak. Some methods of speeding up the convergence of iteration methods. *USSR Computational Mathematics and Mathematical Physics*, 1964. 12
- [46] Chongli Qin, James Martens, Sven Gowal, Dilip Krishnan, Krishnamurthy Dvijotham, Alhussein Fawzi, Soham De, Robert Stanforth, and Pushmeet Kohli. Adversarial Robustness through Local Linearization. *Adv. Neural Inform. Process. Syst.*, 2019. 3
- [47] Haonan Qiu, Chaowei Xiao, Lei Yang, Xinchun Yan, Honglak Lee, and Bo Li. SemanticAdv: Generating Adversarial Examples via Attribute-conditional Image Editing. *arXiv preprint arXiv:1906.07927*, 2019. 3
- [48] Aditi Raghunathan, Sang Michael Xie, Fanny Yang, John Duchi, and Percy Liang. Adversarial training can hurt generalization. In *ICML 2019 Workshop on Identifying and Understanding Deep Learning Phenomena*, 2019. 3
- [49] Benjamin Recht, Rebecca Roelofs, Ludwig Schmidt, and Vaishal Shankar. Do ImageNet Classifiers Generalize to ImageNet? *arXiv preprint arXiv:1902.10811*, 2019. 1
- [50] Leslie Rice, Eric Wong, and J. Zico Kolter. Overfitting in adversarially robust deep learning. *Int. Conf. Mach. Learn.*, 2020. 3
- [51] Evgenia Rusak, Lukas Schott, Roland S. Zimmermann, Julian Bitterwolf, Oliver Bringmann, Matthias Bethge, and Wieland Brendel. A simple way to make neural networks robust against diverse image corruptions. *arXiv preprint arXiv:2001.06057*, 2020. 6
- [52] Yang Song, Rui Shu, Nate Kushman, and Stefano Ermon. Constructing unrestricted adversarial examples with generative models. In *Advances in Neural Information Processing Systems*, pages 8312–8323, 2018. 3
- [53] Masashi Sugiyama, Matthias Krauledat, and Klaus-Robert Müller. Covariate shift adaptation by importance weighted cross validation. *Journal of Machine Learning Research*, 8(5), 2007. 5
- [54] Christian Szegedy, Wojciech Zaremba, Ilya Sutskever, Joan Bruna, Dumitru Erhan, Ian Goodfellow, and Rob Fergus. Intriguing properties of neural networks. *Int. Conf. Learn. Represent.*, 2014. 1, 3
- [55] Rohan Taori, Achal Dave, Vaishal Shankar, Nicholas Carlini, Benjamin Recht, and Ludwig Schmidt. Measuring robustness to natural distribution shifts in image classification. *Advances in Neural Information Processing Systems*, 33, 2020. 2
- [56] Lucas Theis, Wenzhe Shi, Andrew Cunningham, and Ferenc Huszár. Lossy image compression with compressive autoencoders, 2017. 1, 3

- [57] Yuji Tokozume, Yoshitaka Ushiku, and Tatsuya Harada. Between-class learning for image classification. *IEEE Conf. Comput. Vis. Pattern Recog.*, 2018. 2
- [58] Antonio Torralba, Alexei A Efros, and others. Unbiased look at dataset bias. In *IEEE Conf. Comput. Vis. Pattern Recog.*, 2011. 1
- [59] Aäron van den Oord, Oriol Vinyals, and Koray Kavukcuoglu. Neural discrete representation learning. In *Adv. Neural Inform. Process. Syst.*, 2017. 4
- [60] Vladimir Vapnik. *Statistical learning theory*. Wiley New York, 1998. 1
- [61] Igor Vasiljevic, Ayan Chakrabarti, and Gregory Shakhnarovich. Examining the impact of blur on recognition by convolutional networks. *arXiv preprint arXiv:1611.05760*, 2016. 1, 2
- [62] Zhou Wang, Alan C Bovik, Hamid R Sheikh, and Eero P Simoncelli. Image quality assessment: from error visibility to structural similarity. *IEEE transactions on image processing*, 13(4):600–612, 2004. 3, 6, 17
- [63] Eric Wong and J Zico Kolter. Learning perturbation sets for robust machine learning. In *International Conference on Learning Representations*, 2021. 3
- [64] Eric Wong, Leslie Rice, and J. Zico Kolter. Fast is better than free: Revisiting adversarial training. *Int. Conf. Learn. Represent.*, 2020. 6, 12
- [65] Dongxian Wu, Shu-tao Xia, and Yisen Wang. Adversarial weight perturbation helps robust generalization. *Adv. Neural Inform. Process. Syst.*, 2020. 3
- [66] Chaowei Xiao, Bo Li, Jun-Yan Zhu, Warren He, Mingyan Liu, and Dawn Song. Generating adversarial examples with adversarial networks. *arXiv preprint arXiv:1801.02610*, 2018. 3
- [67] Saining Xie, Ross Girshick, Piotr Dollár, Zhuowen Tu, and Kai ming He. Aggregated residual transformations for deep neural networks. *arXiv preprint arXiv:1611.05431*, 2016. 6
- [68] Dong Yin, Raphael Gontijo Lopes, Jonathon Shlens, Ekin D. Cubuk, and Justin Gilmer. A fourier perspective on model robustness in computer vision. *arXiv preprint arXiv:1906.08988*, 2019. 2
- [69] Sangdoon Yun, Dongyoon Han, Seong Joon Oh, Sanghyuk Chun, Junsuk Choe, and Youngjoon Yoo. Cutmix: Regularization strategy to train strong classifiers with localizable features. *Int. Conf. Comput. Vis.*, 2019. 2
- [70] Chiyuan Zhang, Samy Bengio, Moritz Hardt, Benjamin Recht, and Oriol Vinyals. Understanding deep learning requires rethinking generalization. *arXiv preprint arXiv:1611.03530*, 2016. 6
- [71] Hongyi Zhang, Moustapha Cisse, Yann N Dauphin, and David Lopez-Paz. mixup: Beyond empirical risk minimization. *Int. Conf. Learn. Represent.*, 2018. 2
- [72] Hongyang Zhang, Yaodong Yu, Jiantao Jiao, Eric P. Xing, Laurent El Ghaoui, and Michael I. Jordan. Theoretically Principled Trade-off between Robustness and Accuracy. *Int. Conf. Mach. Learn.*, 2019. 3
- [73] Richard Zhang, Phillip Isola, Alexei A Efros, Eli Shechtman, and Oliver Wang. The unreasonable effectiveness of deep features as a perceptual metric. In *CVPR*, 2018. 4

# Appendix

## A. Experimental Setup Details

**Training and evaluation details.** For CIFAR-10 we train pre-activation *ResNet50* [23] models (as in [64]); as in previous work [26] our models use  $3 \times 3$  kernels for the first convolutional layer. We use a standard data augmentation consisting of padding by 4 pixels, randomly cropping back to  $32 \times 32$  and randomly flipping left-to-right.

For IMAGENET we use a standard *ResNet50* architecture for parity with previous works. We use a standard data augmentation, consisting of random left-to-right flips and random crops. We attempt to follow the data-processing setup used by DeepAugment [24]. Due to the increased computational requirements of training models with *AdA* (due to the adversarial training formulation) we resize each random crop (of size  $224 \times 224$ ) to  $128 \times 128$  using bilinear interpolation.

We perform standard evaluation by using the central image crop resized to  $224 \times 224$  on IMAGENET, even though we train models on  $128 \times 128$  crops.

**Outer minimization.** We minimize the corrupted adversarial risk by optimizing the classifier’s parameters using stochastic gradient descent with Nesterov momentum [45, 41]. For CIFAR-10 we train for 300 epochs with a batch size of 256 and use a global weight decay of  $10^{-4}$ . For IMAGENET we train for 90 epochs with a batch size of 4096 and use a global weight decay of  $5 \cdot 10^{-4}$ . We use a cosine learning rate schedule [38], without restarts, with 5 warm-up epochs, with an initial learning rate of 0.1 which is decayed to 0 at the end of training. We scale all learning rates using the linear scaling rule of [19], i.e., effective LR =  $\max(\text{LR} \times \text{batch size}/256, \text{LR})$ .

**Inner maximization.** Corrupted adversarial examples are obtained by maximizing the cross-entropy between the classifier’s predictions on the corrupted inputs (by passing them through the corruption network) and their labels. We initialize the perturbations to the corruption network parameters randomly within the feasible region. We optimize the perturbations using iterated FGSM steps [16, 33]<sup>7</sup>. We project (i.e., clip) the optimization iterates to stay within the feasible region. We use a step size equal to 1/4 of the median perturbation radius over all parameter blocks (for each backbone network individually). For CIFAR-10 we use 10 steps; for IMAGENET we use only 3 steps (due to the increased computational requirements) but we increase the step size by a factor of 10/3 to compensate for the reduction in steps. When *AdA* is specified to use both backbones (e.g., as “*AdA* (EDSR, CAE)”) each backbone is used for finding adversarial examples for half of the examples in each batch.

**Combining data augmentation methods.** We view the process of combining data augmentation methods as a data pipeline, where the output from each stage is fed as input to the next stage. We first draw random samples either from the clean training dataset, or from the DeepAugment-processed training set if DeepAugment is used (this is how DeepAugment is used in the original paper [24]). Then we apply standard data augmentation (random pad and crop for CIFAR-10, random left-right flip and resized crop for IMAGENET). On IMAGENET we resize the standard  $224 \times 224$  crop to  $128 \times 128$ . If *AdA* is used, we apply the method now in the pipeline (followed by the SSIM line-search procedure). If AugMix is used, on CIFAR-10 we apply it as the final step in the data pipeline. On IMAGENET we apply AugMix before *AdA* instead; this is motivated empirically, as we observed that we can obtain slightly better results (by approximately 1% mCE) by using this ordering.

## B. Performance under Stochastic Parameter Perturbations

In this section we provide experimental support for the PAC-Bayes analysis in section 4 of the main manuscript. Specifically, in Table 5, we show that the performance of an *AdA*-trained classifier gradually degrades under increasingly larger perturbations to its parameters.

Let  $w$  denote a block of parameters (e.g., the set of convolutional filters of a layer) and  $w_j$  be the  $j$ -th coordinate of the parameter block; then,  $\epsilon_j$  is the stochastic perturbation we add to the individual scalar parameter  $w_j$ . We draw the perturbation  $\epsilon_j$  from a 0-mean Gaussian with standard deviation proportional to the  $\ell_\infty$  norm (i.e., the maximum absolute value) of the enclosing parameter block:  $\epsilon_j \sim \mathcal{N}(0, \eta \|w\|_\infty)$ , where  $\eta$  denotes the standard deviation scaling factor. We vary  $\eta$  from 0.00 (0% noise; i.e., nominally evaluated model) to 0.10 (10% noise) in increments of 0.02 (2% noise at a time), as shown in the

<sup>7</sup>We also experimented with Adam, SGD and normalized gradient ascent but we obtained the best results using FGSM.

first column of Table 5. We sample stochastic parameter perturbations (for all of  $f_\theta$ 's parameters) 50 times per dataset example and average the model's predicted probabilities (i.e., we average the softmax predictions and then compare the averaged prediction with the ground-truth label).

We observe a gradual degradation in mCE and clean error when increasing the expected magnitude of parameter perturbations. Performance on mCE is maintained up to and including a noise level of 2%, and on clean error up to a noise level of 4% respectively.

Table 5: **Robustness to common image corruptions under stochastic parameter perturbations.** The table shows top-1 clean error, mCE and individual corruption error (averaged over all severities) for increasingly larger stochastic parameter perturbations to the *AdA* + AUGMIX classifier trained on CIFAR-10.

NOISE (%)	CLEAN E	MCE	NOISE			BLUR				WEATHER				DIGITAL			
			GAUSS	SHOT	IMPULSE	DEFOCUS	GLASS	MOTION	ZOOM	SNOW	FROST	FOG	BRIGHT	CONTRAST	ELASTIC	PIXEL	JPEG
0% (default)	<b>3.74%</b>	<b>8.80%</b>	16.4	12.8	14.4	5.7	10.9	7.5	6.3	7.7	6.7	6.6	3.9	4.7	8.1	11.9	8.4
2%	3.76%	8.81%	16.5	12.8	14.5	5.7	10.9	7.6	6.4	7.7	6.7	6.6	3.9	4.8	8.1	11.8	8.3
4%	3.75%	9.21%	17.4	13.4	15.2	6.2	11.4	8.2	6.9	7.9	6.9	6.8	4.0	5.6	8.2	11.7	8.3
6%	4.28%	10.49%	19.5	15.1	17.2	7.3	12.8	9.8	8.5	8.6	7.7	7.8	4.4	8.5	9.0	12.4	8.9
8%	6.01%	14.56%	24.5	19.4	22.9	11.2	17.9	14.7	12.6	11.6	10.1	11.3	6.4	15.8	12.3	16.2	11.4
10%	17.75%	31.34%	40.7	35.5	44.5	26.9	40.9	34.5	30.2	29.0	22.2	24.9	19.2	34.2	28.2	32.8	26.2

### C. Approximate SSIM line-search procedure

The adversarial examples produced by *AdA* can sometimes become too severely corrupted (i.e., left-tail of densities in Figure 2 of the main manuscript). We guard against these unlikely events by using an efficient, approximate line-search procedure. We set a maximum threshold, denoted by  $t$ , on the SSIM distance between the clean example and the *AdA* adversarial example.

Denote by  $x_\gamma$  the linear combination of the clean example,  $x$ , and the corrupted example output by *AdA*,  $\hat{x}$ :

$$x_\gamma = (1 - \gamma)x + \gamma\hat{x}.$$

When the deviation in SSIM between the clean and the corrupted example is greater than the threshold ( $\text{SSIM}(x, \hat{x}) > t$ ), we find a scalar  $\gamma^* \in [0, 1]$  such that the deviation between the corrected example,  $x_{\gamma^*}$ , and the clean example,  $x$ , is  $t$ :  $\text{SSIM}(x, x_{\gamma^*}) = t$ . We take 9 equally-spaced  $\gamma$  values in  $[0, 1]$  and evaluate the SSIM distance between the clean example and  $x_\gamma$  for each considered  $\gamma$ . We fit a quadratic polynomial in  $\gamma$  to all the pairs of  $\gamma$  and the threshold-shifted SSIM deviation from the clean example  $\text{SSIM}(x, x_\gamma) - t$ . We then find the roots of this polynomial, clip them to  $[0, 1]$ , and take the  $\gamma$  closest to 1 as the desired  $\gamma^*$ . This corresponds to returning the most corrupted variant of  $x$  along the ray between  $x$  and  $\hat{x}$  which obeys the SSIM threshold. The procedure is very efficient on accelerators (GPUs, TPUs) as it requires no iteration. It is approximate however because the quadratic polynomial sometimes underfits.

### D. Additional Experiments and Comparisons

**Comparison to Vanilla and Perceptual Adversarial Training on CIFAR-10.** Perceptual Adversarial Training (PAT) [34] proposes an adversarial training method based on bounding a neural perceptual distance (LPIPS). Appendix G (Table 10) of the PAT article shows the performance of various models on common image corruptions. However, performance is summarized using *relative* mCE, whereas we use *absolute* mCE throughout. The authors kindly provided us<sup>8</sup> with the raw corruption errors of their models at each severity and we reproduce their results in (the top half of) Table 6. We observe that PAT has overall lower robustness to common image corruptions (best variant obtains 23.54% mCE) than AugMix (10.90% mCE) and than our best *AdA*-trained model (7.83% mCE).

PAT however, performs very well against other adversarial attacks<sup>9</sup>, including  $\ell_p$ -norm bounded perturbations. The best PAT model obtains 28.7% robust accuracy against  $\ell_\infty$  attacks ( $\epsilon = 8/255$ ) and 33.3% on  $\ell_2$  attacks ( $\epsilon = 1$ ) while our best

<sup>8</sup>Personal communication.

<sup>9</sup>See Table 2 of [34] for full details.

*AdA*-variant obtains less robust accuracy in each case (0.99% against  $\ell_2$  attacks and 13.88% against  $\ell_\infty$  attacks with  $\epsilon = 4/255$ ). This difference in performance against  $\ell_p$ -norm attacks is not surprising, as PAT addresses robustness to pixel-level attacks (i.e., it manipulates image pixels directly); whereas *AdA* applies adversarial perturbations to the corruption function parameters (and not to the image pixels directly).

In similar spirit to PAT, [30] introduce an efficient relaxation of adversarial training with LPIPS as the distance metric. Their best model, with a smaller architecture, RESNET18, obtains 11.47% mCE on CIFAR-10-C.

The authors of [30] also show that models trained adversarially against  $\ell_p$ -norm bounded perturbations can act as a strong baseline for robustness to common image corruptions. The strongest known<sup>10</sup> adversarially trained model against  $\ell_p$ -norm bounded perturbations on common image corruptions is that of [18] which obtains 12.32% mCE (training against  $\ell_2$ -norm bounded perturbations with  $\epsilon = 0.5$  while using extra-data).

To the best of our knowledge, our best performing model is more robust to common image corruptions on CIFAR-10 than all previous methods, obtaining a new state-of-the-art mCE of 7.83%.

**Table 6: Performance of Perceptual Adversarial Training on common image corruptions.** The table lists the performance of *ResNet50* models trained using Perceptual Adversarial Training by the original authors of [34] on common image corruptions and two of our *AdA*-trained models. The table shows clean error, mean corruption error on CIFAR-10-C and individual corruption errors for each corruption type (averaged across all severities). “PAT-self” denotes the case where the same model is used for classification as well as for computing the LPIPS distance, while “PAT-AlexNet” denotes the case where the LPIPS distance is computed using a pre-trained CIFAR-10 AlexNet [31] classifier.

SETUP	CLEAN E	MCE	NOISE			BLUR				WEATHER				DIGITAL			
			GAUSS	SHOT	IMPULSE	DEFOCUS	GLASS	MOTION	ZOOM	SNOW	FROST	FOG	BRIGHT	CONTRAST	ELASTIC	PIXEL	JPEG
<b>PAT MODELS [34]</b>																	
Nominal Training	5.20%	25.80%	54.0	42.0	38.0	16.0	50.0	21.0	21.0	18.0	24.0	10.0	6.0	16.0	17.0	28.0	20.0
Adversarial Training $\ell_\infty$	13.20%	20.71%	18.0	17.0	22.0	16.0	19.0	20.0	17.0	17.0	18.0	32.0	13.0	47.0	18.0	15.0	15.0
Adversarial Training $\ell_2$	15.00%	21.83%	18.0	17.0	21.0	18.0	20.0	21.0	18.0	19.0	20.0	35.0	16.0	47.0	20.0	16.0	16.0
PAT-self	17.60%	23.54%	22.0	21.0	25.0	20.0	22.0	22.0	20.0	23.0	23.0	33.0	19.0	38.0	21.0	18.0	19.0
PAT-AlexNet	28.40%	34.25%	33.0	31.0	36.0	30.0	34.0	33.0	32.0	33.0	35.0	43.0	30.0	46.0	32.0	29.0	29.0
<b>SELECTION OF <i>AdA</i> MODELS (OURS)</b>																	
<i>AdA</i> (EDSR)	3.82%	12.49%	25.0	19.0	29.0	9.0	15.0	10.0	9.0	9.0	8.0	8.0	4.0	11.0	9.0	6.0	9.0
<i>AdA</i> (EDSR) + DeepAugment (10×) + AugMix	5.07%	7.83%	8.0	7.0	11.0	5.0	10.0	7.0	6.0	8.0	6.0	8.0	5.0	6.0	8.0	7.0	7.0

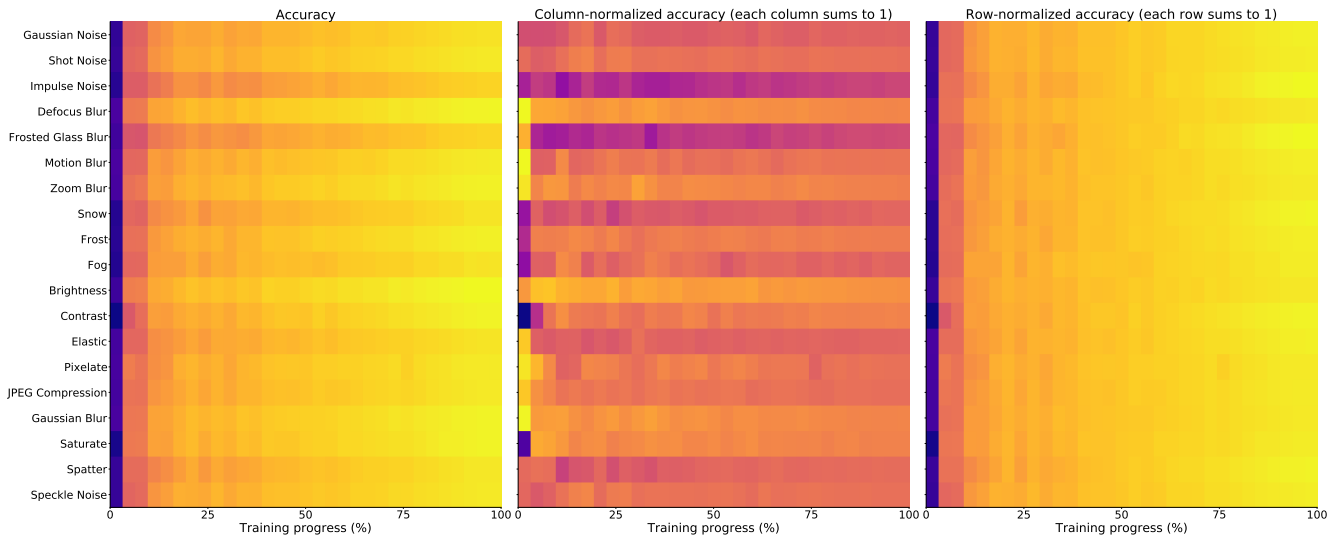
**Performance on image corruptions through training.** We visualize the performance of *AdA* trained models (best *AdA*-combination from Table 1 and Table 3 from the main manuscript) during training in Figure 4. Due to adversarial training, we expect the performance on each of the \*-C corruptions to improve as training progresses, and this is indeed what we observe. On both datasets, the *AdA*-trained classifiers perform consistently best on *Brightness*, especially at the beginning of training. On IMAGENET performance increases more slowly on the *Blur*-type corruptions than on all others.

**Reconstructing CIFAR-10-C corruptions through *AdA* backbones.** We include the full variant of Figure 3 (from the main manuscript) in Figure 5. The figure shows how well can each one of the corruptions of CIFAR-10-C be approximated by the corruption functions (*EDSR* and *CAE*) used by *AdA*.

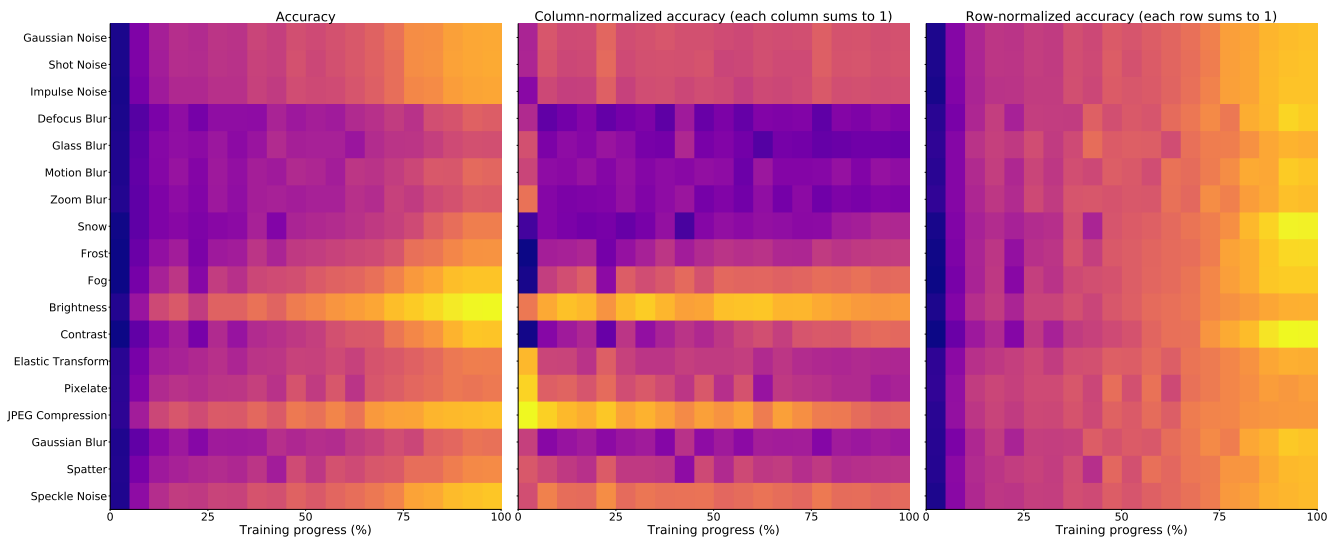
**Additional results on IMAGENET.** We provide supplemental results to Table 3 (from the main manuscript) on robustness to common image corruptions in Table 7. Specifically, we include additional results for *AdA* variants without AugMix. We note that AugMix helps improve robustness performance when paired with any other model.

**Ablation on *AdA* perturbation radius.** We show the effect of changing the corruption network parameters perturbation radius in *AdA* on CIFAR-10 in Table 8. We perform a sweep on the perturbation radius by scaling the radius ( $\nu = 0.015$ ) of the best performing model, *AdA* (EDSR) + DEEPAUGMENT (10×) + AUGMIX (from Table 1 in the main manuscript), by {0.5, 0.75, 1.0, 1.25, 1.5}. We observe that the robustness performance varies minimally across a small range of perturbation radii.

<sup>10</sup>See the ROBUSTBENCH [8] leaderboard: <https://robustbench.github.io>.



(a) CIFAR-10



(b) IMAGENET

**Figure 4: Performance on image corruptions through training.** These plots visualize the performance of the best *Ada* combination on each of the common and extra \*-C corruptions as training progresses. Each individual rectangle plots top-1 accuracy. Brighter is better. The accuracies are visualized raw (plots to the left), normalized over the columns (middle plots) or over the rows (plots to the right). Normalizing over the columns visualizes which corruption’s performance is best at that point in training. Normalizing over the rows visualizes at which stage the classifier performs best on a given corruption.

Table 7: **Robustness to common image corruptions (IMAGENET-C 128×128)**. The table shows mean corruption error on IMAGENET-C and individual corruption errors for each corruption type (averaged across all severities).

SETUP	MCE	NOISE			BLUR				WEATHER				DIGITAL			
		GAUSS	SHOT	IMPULSE	DEFOCUS	GLASS	MOTION	ZOOM	SNOW	FROST	FOG	BRIGHT	CONTRAST	ELASTIC	PIXEL	JPEG
<i>AdA (EDSR, CAE) + DeepAugment + AugMix</i>	<b>67.36%</b>	48.3	48.1	48.9	62.7	65.7	60.9	63.0	55.9	<b>52.0</b>	44.0	36.4	44.1	56.0	<b>56.8</b>	44.8
<i>AdA (EDSR, CAE) + DeepAugment</i>	68.77%	<b>47.5</b>	<b>48.0</b>	<b>48.5</b>	63.5	<b>65.3</b>	63.1	65.1	56.0	52.1	47.6	35.4	53.8	54.0	57.6	47.2
<i>AdA (EDSR, CAE) + AugMix</i>	72.23%	61.6	61.1	64.7	66.0	69.0	60.3	60.8	58.0	55.6	41.3	33.4	<b>41.1</b>	54.0	60.3	60.2
<i>AdA (EDSR, CAE)</i>	78.02%	71.3	71.3	77.3	68.8	71.0	65.2	64.3	61.5	57.2	45.8	34.4	57.0	55.5	63.9	57.0
<i>AdA (EDSR) + AugMix</i>	73.59%	67.3	68.2	71.7	65.6	73.8	62.8	61.1	61.3	58.7	39.8	<b>31.9</b>	43.2	55.6	60.8	48.5
<i>AdA (EDSR)</i>	79.59%	74.9	75.4	78.0	70.1	75.0	67.9	66.3	62.9	60.0	44.4	33.6	56.7	57.4	64.8	54.9
<i>AdA (CAE) + AugMix</i>	80.85%	87.4	86.6	91.2	66.7	65.7	63.0	63.0	71.3	66.0	50.6	42.2	52.2	<b>53.3</b>	59.1	<b>44.8</b>
<i>AdA (CAE)</i>	86.44%	89.6	89.2	94.4	75.8	70.3	68.3	66.8	75.5	68.3	56.4	45.1	65.3	55.1	62.1	47.8
DeepAugment	73.04%	52.1	52.1	53.3	60.5	69.0	65.9	63.3	57.7	55.4	43.8	33.8	58.2	56.2	66.8	63.8
DeepAugment + AugMix	70.05%	50.5	50.0	51.5	<b>58.0</b>	67.8	<b>60.1</b>	<b>58.1</b>	<b>54.5</b>	53.3	<b>37.5</b>	33.4	43.6	56.3	64.2	72.0
AugMix	77.12%	70.4	71.6	75.6	67.2	75.1	64.0	59.0	60.9	61.1	37.9	34.7	46.9	57.5	71.4	55.9
Nominal	82.40%	73.3	74.8	80.1	71.4	78.5	70.4	65.1	66.7	63.6	46.1	35.8	63.3	57.4	72.4	55.9

Table 8: **Effect of perturbation radius on robustness to common image corruptions (CIFAR-10-C)**. The table shows the performance of the best *AdA*-combination from Table 1 from the main manuscript (*AdA (EDSR) + AUGMIX + DEEPAUGMENT*) while varying the perturbation radius ( $\nu$ ). The table shows mean corruption error on CIFAR-10-C and individual corruption errors for each corruption type (averaged across all severities).

PERTURBATION RADIUS	MCE	NOISE			BLUR				WEATHER				DIGITAL			
		GAUSS	SHOT	IMPULSE	DEFOCUS	GLASS	MOTION	ZOOM	SNOW	FROST	FOG	BRIGHT	CONTRAST	ELASTIC	PIXEL	JPEG
$\nu = 0.0225$	8.10%	9.4	8.1	11.5	6.2	11.4	7.5	6.6	8.8	6.9	<b>8.5</b>	5.5	6.4	8.8	7.8	8.1
$\nu = 0.01875$	8.06%	8.8	7.9	11.5	6.1	11.2	7.6	6.5	9.0	7.0	8.7	5.5	6.5	8.8	7.6	8.1
$\nu = 0.015$ (default)	<b>7.83%</b>	<b>8.8</b>	<b>7.8</b>	11.2	<b>5.9</b>	<b>10.7</b>	<b>7.3</b>	6.5	<b>8.5</b>	<b>6.7</b>	8.7	<b>5.2</b>	<b>6.2</b>	<b>8.5</b>	7.7	<b>7.8</b>
$\nu = 0.01125$	8.41%	9.1	8.3	12.1	6.5	11.3	8.0	6.8	9.2	7.2	9.2	5.8	6.8	9.2	8.1	8.5
$\nu = 0.0075$	7.99%	8.9	8.0	<b>11.0</b>	6.2	10.7	7.7	<b>6.2</b>	9.0	6.9	8.6	5.5	6.9	8.7	<b>7.6</b>	8.1



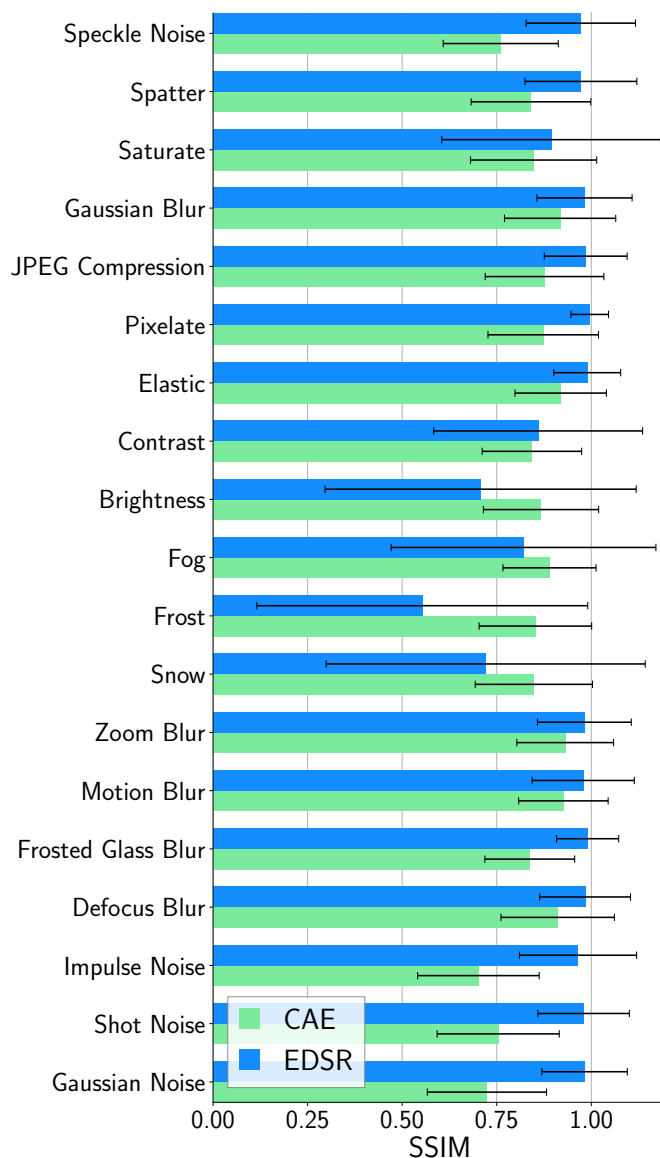


Figure 5: **Reconstructing CIFAR-10-C corruptions through Ada backbones.** These bar plots show the extent to which the *EDSR* and *CAE* models can be used to approximate the effects of all the corruptions present in CIFAR-10-C. Bars show mean and std. dev. SSIM [62] (higher is better, 1 is max.) between pairs of corrupted images and their reconstructions through *EDSR/CAE*, optimized starting from the corresponding clean images.